Concentric photothermal coagulation with basket-integrated optical device for treatment of tracheal stenosis

Van Nam Tran,[1†] Hyungshin Lee,[2†] Van Gia Truong,[1] Yun-hee Rhee,[3] and Hyun Wook Kang[1,4,]*

[†]The authors contributed equally to this work

*wkang@pukyong.ac.kr

[1]Department of Biomedical Engineering, Pukyong National University, Busan 48513, Korea
[2]Department of Otolaryngology Head and Neck Surgery, Kosin University, Busan 49267, Korea
[3]Beckman Laser Institute Korea, Dankook University, Cheon-an 31116, Korea
[4]Center for Marine-Integrated Biomedical Technology, Pukyong National University, Busan 48513, Korea

Keywords: basket, optical diffuser, circumferential coagulation, tracheal stenosis

Short title: V. N. Tran et al.: Concentric photothermal coagulation with basket device for tracheal treatment

A basket-integrated optical device is developed to consistently treat tubular tissue by centering an optical diffuser in the lumen. Four nitinol arms in conjunction with the optical diffusing applicator are deployed to induce homogeneous circumferential light emission and concentric photothermal coagulation on tracheal tissue. 1470-nm laser light is employed for the tissue testing at various irradiation conditions and evaluated in terms of thermal gradient and temperature evolution. Preliminary experiments on liver tissue demonstrate the concentric development of the radial thermal coagulation in the tissue (eccentric ratio = ~5.5 %). The interstitial tissue temperature increases with the total amount of energy delivery (around 65 ˚C). *Ex vivo* trachea testing yields up to 16.5% tissue shrinkage due to dehydration as well as uniform ablation of the cilia and goblet cells in a mucosa layer under 7-W irradiation for 10 s. The proposed optical device may be a feasible therapeutic method to entail the circumferential coagulation in the tubular tissues in a reliable manner.

This article has been accepted for publication and undergone full peer review but has not been through the copyediting, typesetting, pagination and proofreading process, which may lead to differences between this version and the Version of Record. Please cite this article as doi: 10.1002/jbio.201700073

1. Introduction

Trachea, also called as windpipe, allows air passing through the pharynx and larynx to the lungs. Tracheal stenosis, consisting of subglottic stricture, is thereby an airway narrowing phenomenon that can take place due to the prolonged intubating procedures, tracheostomy surgery, trauma, inflammation and infection conditions (tuberculosis), tumors, malignancy (primary or metastatic) and other systematic diseases [1-5]. According to the previous study [6], 54.7% of tracheal stenosis patients experienced an iatrogenic etiology, followed by idiopathy (18.5%), autoimmunity (18.5%), and traumatic causes (8%). In particular, the incident percentage of patients who are susceptible to tracheal obstruction after intubation and tracheostomy accounted for 6% - 21% and 0.6% - 21%, respectively [7]. In Korea, endotracheal intubation can be seen as the most common etiology of tracheal stenosis [8]. Tracheal stricture symptoms and signs are relatively obvious as patients typically show wheezing, coughing or shortly and hardly breathing (severe dyspnea). Additionally, a high-pitched squeal occurs during inhaling or the skin color becomes slightly blue.

Depending on each specific grade of tracheal stenosis, patients may be suggested with different therapeutic strategies. In recent years, some tracheal treatment methods have been introduced such as stent insertion [9, 10], prolonged endotracheal intubation [3, 11], resection and reconstruction [12, 13], and laser surgery [2, 14]. Although tracheal stenting has advantages of minimally invasive effect, a shorter period of anesthesia, and ability to access to the entire intrathoracic trachea, the stent irritates the trachea, resulting in many unexpected side effects post-operatively. The tracheal dilation is able to shortly enlarge the windpipe, and the clinical result usually lasts around 6 months after the surgery; however, mechanical dilation may cause a high rate of mortality and more than 90% of treated trachea can encounter recurrence [15]. While tracheal resection and reconstruction are typically considered a standard treatment procedure for most patients, the fact remains that it is an invasive surgery, which thus requires an additional anesthetic and hemostatic procedure [12,

16]. Lasers have been applied for many medical areas including severe tracheal treatment due to minimally invasive procedures and controllable optical penetration depth (consistent coagulation), leading to effective short-term results and temporary relief. A number of laser types have been effectively and efficiently used such as Nd: YAG (1064 nm), thulium fiber laser (1940 nm), KTP (532 nm) and CO_2 (10.6 μm) lasers [8, 14, 17, 18]. In particular, many scientists have been using optical diffusing fibers to either induce stricture or treat stenosis in tubular tissue such as varicose veins [19], urethra [20], seminal duct [21], trachea in rabbits [2]. However, it is relatively difficult to insert and position the laser device at the right center of lumen to induce a circumferentially homogeneous coagulation in the tissue walls. Conceivably, the clinical outcomes can depend on personal skills and experiences, which are different from one to the other. Balloon catheters have been successfully employed to center optical fibers for photodynamic therapy (PDT) [22]. Nonetheless, balloon pressure on the targeted tissue surface could possibly reduce blood flow and oxygenation, adversely affecting treatment outcomes [23, 24]. In fact, plastic balloon catheters should not be deployed with infrared laser light due to high light absorption and melting phenomena. Therefore, a basket device in conjunction with optical diffusing applicator was designed and developed to achieve concentric thermal treatment on tracheal tissue.

2. Materials and Methods

2.1. Design of basket-integrated device

The main purpose of integrating a basket device was to position an optical diffuser in the center of tubular tissue with a flexible lumen size during photothermal treatment in order to achieve uniform thermal coagulation around the tissue wall. For direct tissue contact, the basket device was needed to expand the tissue lumen in a reliable manner and to have mechanical integrity during the operation. Figure 1 shows the conceptual design of the basket-assisted optical device for the current study. The device consisted of a conical head, four wire arms, an optical diffuser, a conveyer, a medical plastic tube, and a push-pull handle. 0.3-mm diameter nitinol with a stoichiometric ratio of Ti:Ni = 1:1 (HTTS 65785, Sarah Zhang company, Shaanxi, China) was used for the four wire arms due to two unique behaviors: pseudo-elasticity and shape memorization [25-31]. In addition, the nitinol material has demonstrated excellent biocompatibility and similar mechanical response to biological tissues [32-34]. As the plastic outer sheath with an outer diameter (OD) of 3.2 mm (1648L, IDEX Health & Science LLC, WA, USA) was pulled in by using the customized handle, the nitinol arms became self-expandable and directly contacted the inner wall of the tubular tissue. The four contact areas also provided strong mechanical integrity to maintain the position of the diffuser at the center of the tissue lumen (self-centering). PCNC machine (PCNC 440, Tormach Inc, Waunakee, WI, USA) was employed to make a customized mold to shape each wire arm in the predetermined geometry and dimensions. Each arm was initially cut into a segment of 20 mm and firmly positioned in the mold. Then, the arms were annealed in the uniform temperature environment at around 500 ^{0}C induced by a hot air gun (SKIL 8006, Skil Europe B.V. Konijnenberg, Breda, Netherlands). After 5 minutes annealing, the four arms were removed from the mold and put into cold water to render their phase state stable. Due to intrinsic thermal properties, the nitinol arms were able to memorize the predetermined shape and dimensions [25, 35]. To ensure performance reliability, each arm was straightened for 24

hours and its shape was repeatedly measured and evaluated until no changes in shape and dimension were confirmed. Therefore, the four arms could operate reliably and accurately during the operation. The outer diameter of plastic conical head was designed to fit with the outer sheath of the plastic tube (OD = 3.2 mm). On the proximal cross-section of the head, four holes (inner diameter, ID = 0.4 mm) were drilled to fix the four wire arms by using optical adhesive exposed to UV light (λ = 365 nm). Moreover, its distal tip was fabricated in conical shape to ease the insertion process. An additional function of the cap was to coaxially fix the optical diffuser with the four wire arms. Similar to the conical cap, the plastic conveyer was fabricated as a long cylinder (length = 5 mm, OD = 2.4 mm, and ID = 1 mm) to fit into the inner wall of the tube, and thus, the optical diffuser was always positioned along the plastic tube direction. Prior to the irradiation, the plastic conveyer was completely pulled back to ensure no light interaction, and the diffusing light merely interacted with tissue lumen.

After the fabrication of the basket device, an optical diffuser was prepared to distribute light in a cylindrical manner. A multimode 600-μm core diameter (FT600EMT, Thorlabs Inc., Newton, New Jersey, USA) was machined by using a 60-W CO_2 laser system (λ = 10.6 μm, Synrad, Mukilteo, WA, USA). After being cleaned with methanol liquid, the bare fiber was initially mounted on fiber chucks, and fabrication movements were controlled by using LabView software (National Instruments Corporation, Austin, Texas, USA). Helical patterns were thus grooved on the fiber surface (10-mm active length) to attain circumferential light distribution. A customized glass cap (inner diameter = 1 mm, thickness = 0.2 mm, and length = 16 mm) was then added to the fabricated tip to prevent any mechanical damage and then sealed by using optical adhesive exposed to UV light (λ = 365 nm). Spatial distribution of light intensity (radial and longitudinal directions) from the fabricated diffuser was experimentally measured by using a customized goniometric system in conjunction with a photodiode (PD-300-3W, Ophir, Jerusalem, Israel). Due to the limited spectral range of the photodiode (350 ~ 1100 nm), HeNe light (λ = 632 nm) was instead employed for the entire

emission measurements. The photodiode received the diffused HeNe light through a collimated tube with an inner diameter of 1 mm. The fiber was fixed on adjustable mounts and controlled by using LabView software. For radial emission measurements, the optical diffuser was vertically mounted, and the sensor was rotated around the axis of the diffuser at the middle point of the diffusing segment (5 mm from proximal end). For longitudinal emission measurements, the diffuser was horizontally positioned, and the sensor was moved along with the axis of the diffuser from the distal to the proximal (0.3 mm/s). The measured radial and longitudinal intensities were normalized to minimize any effect of laser power fluctuations on the measurements. To validate the goniometric results, the longitudinal HeNe light distribution from the diffuser was also captured by using a digital camera (Canon-70D-18-55, Canon Park, Melville, NY, USA). ImageJ software was then used to measure a 1-cm long intensity profile of the diffusing part from the captured image along the fiber axis. The acquired intensity data were then digitized, and data analysis software (Origin 8.0, OriginLab, Northampton, MA, USA) was employed to filter the data to remove low-pass signals and to smooth out the intensity profile for comparative analysis. To confirm the total power transmitted from the diffuser, an integrating sphere (IS200-4 - Ø2", Thorlabs Inc., Newton, New Jersey, USA) in conjunction with a spectrometer (FLAME-S-VIS-NIR-ES, Ocean Optics, Inc., Dunedin, FL 34698, USA) was employed.

Finally, both the basket device and the optical diffuser were integrated coaxially (Fig. 1). For the device expansion, the head of the basket was pushed forward through the plastic sheath until four nitinol arms were fully expanded in a memorized shape. The outer diameter of the expanded four arms was selected to be 6 mm to fit the lumen of tubular trachea which was ranging from 5 to 6 mm in the current experiment. Therefore, the optical fiber was firmly positioned in the center of the trachea lumen with no mechanical deformation in the trachea based upon endoscopic observations.

2.2. Mechanical validation of the basket device

In order to test structural integrity of the fabricated basket device, the extent of radial compression was quantitatively evaluated by using a digital push-pull force gauge HF-50 N (M&A Instruments Inc., ARCADIA, CA). The basket device was horizontally positioned between the gauge arm and a fixed steel plate. The radial force (P) was measured as a function of radial displacement, and the radial stiffness (K_r) was defined as a ratio of P applied to the outer surface of the basket to radial decrease (Δr) of the basket (i.e., $K_r = P/\Delta r$). The device was radially compressed in each displacement of 0.1 mm until both the top and the bottom arms almost touched the fiber glass cap (total displacement = 4 mm). Cyclic loading was also applied to evaluate recovery capacity (super-elasticity and shape memory) of the basket after occlusion. The experiments were repeated five times for each pair of the four wire arms ($N = 5$).

2.3. Evaluation of coagulation eccentricity

In order to demonstrate centering capability of the proposed device, an experiment was conducted on bovine liver tissue. Two groups were tested for assessing coagulation eccentricity (N = 15 per group): one group used only with an optical applicator and the other group with the basket-integrated optical applicator. Due to high light absorption by water, a 1470-nm diode laser system (FC-W-1470, CNI, Changchun, China) was employed at the treatment dosage of 7 W and 10 s (total energy = 70 J) to steadily induce thin coagulation layers without deep thermal damage to the peripheral tissue [2]. The liver samples were harvested from a local abattoir and kept at -15 °C for an hour. Each frozen sample was prepared in a size of 30×30×30 mm^3 (i.e., volume = 27 cm^3). A 5-mm hole was then drilled in each frozen liver by using a circular clay hole cutter (OD = 5 mm) to replicate a hollow lumen of tubular trachea. All the prepared samples were preserved at 20 °C prior to the testing. In each group, either optical diffuser or basket device was longitudinally positioned along the

axis of the tissue lumen. Irreversible thermal coagulation was visibly determined by discoloration on the sample surface. During laser irradiation, an infrared camera (8-cm focal length macro-lens, **320×240 pixels**, and resolution = 25 μm; A300, FLIR, Winsonville, OR) with a spectral range of 7.5~13 μm was used to monitor the surface temperature, which indirectly assessed coagulation development in the tissue. **Before the treatment, liver emissivity (0.98) was referred to calibrate the camera according to the instructions from the manufacturer's manual [36, 37].** After the treatment, the liver samples were preserved at -15 ^{0}C for an hour and cross-sectioned for further analysis. Then, the surface of the coagulated tissues was photographed, and the degree of the thermal coagulation was evaluated by using ImageJ software (National Institute of the Health, Bethesda, MD) for quantitative comparison. Eccentricity (e) was evaluated to identify how thermal coagulation was distributed around the drilled hole in the tissue. Two fitting circles for the drilled hole and the coagulation circumference were initially created on each captured tissue image. ImageJ was used to estimate e by measuring the distance between the centers of the hole and the coagulation circumference (N = 5). Statistical analysis (Student's t-test) was conducted by using SPSS program (SPSS Inc., Chicago, IL, USA), and $p < 0.05$ was regarded as significant [1]. In order to evaluate the degree of the coagulation eccentricity, the ratio (e/R_0, where R_0 is the radius of the drilled hole = 2.5 mm) was calculated by using their mean values. As the smaller ratio represents the better concentric treatment, the ratio less than 10% was considered instrumental in ensuring the uniform thermal coagulation in the tubular tissue.

2.4. Trachea experiment with basket device

Figure 2 demonstrates an experimental set-up of *ex vivo* trachea testing. The rabbit trachea tissue was procured from a local animal center after animals were euthanized for other experiments. Each tissue was then cut in the segment of 20 mm and stored in saline at 4 °C

prior to the experiment to avoid dehydration and structural deformation. The basket device was horizontally fixed on adjustable mounts in the region of interest (ROI) and was inserted into the trachea tissue. Similar to liver experiments, a 1470-nm diode laser system was employed for tissue coagulation with a basket-integrated optical applicator due to strong light absorption by water in the trachea. Prior to the thermal treatment, HeNe laser beam was used to exactly navigate the tissue position on the basket. An IR camera was positioned around 8 cm above the sample and used to monitor the temperature development of the outer tissue surface at various irradiation conditions to indirectly evaluate the coagulation process. **Both a thin slice of trachea and a black electrical tape (emissivity = 0.97) with the same temperature were deployed to determine the emissivity of trachea tissue (~ 0.98) for the purpose of the camera calibration [37].** The temporal elevation of the temperature was assessed from a single point of the tissue surface (middle position). In addition, the spatial distribution of the temperature was validated along the axis of the tissue lumen (longitudinal direction) at the end of the laser irradiation. Transient temperature increase rates were then evaluated by dividing the temperature increase by the corresponding irradiation time **(i.e., total time to reach maximum temperature).** A digital camera (Canon-70D-18-55, Canon Park, Melville, NY, USA) was located below the sample to capture the images of the treated tissue, and a neutral filter was situated in-between to avoid any intensity saturation during the laser irradiation. All the data acquired from the IR and the digital cameras were collected and transferred to a computer for post-experimental analysis. According to *in vivo* rabbit model of trachea stenosis classification [2], the current study tested three conditions (power - time - energy): 7 W–5 s–35 J, 7 W–10 s–70 J, and 10 W–5 s–50 J. Each condition was repeated five times (N = 5). The initial tissue diameter (i.e., diameter before treatment; D_i) and the final tissue diameter (i.e., diameter after treatment; D_f) were measured by using ImageJ to evaluate the spatial shrinkage ($\Delta D = D_i - D_f$) due to dehydration (N = 5). All the samples were then fixed in formalin and later prepared for histology slides. Each specimen was sliced into 4-µm

thickness and stained with hematoxylin and eosin, then analyzed by using an optical transmission microscope (ICC50 HD, Leica Camera AG, Wetzlar, Germany) to confirm cell shrinkage and extracellular vacuolization phenomenon due to dehydration in the water-dominated tissue under the 1470-nm laser irradiation.

3. Results

3.1. Light distribution comparison

Figure 3 illustrates the normalized beam profiles of an optical diffuser in longitudinal and radial directions. In Fig. 3(a), the dark red line exhibits the emission profile measured by a goniometric system while the blue line represents the profile acquired from the processed digital image. Overall, the longitudinal light distribution was **almost** symmetric and homogeneous **(i.e., uniform light intensity at fixed distance from diffuser surface)** although the proximal intensity was 20% higher than the distal one. It should be noted that both the profiles demonstrated a very similar trend from the proximal end to the distal end apart from a minor difference at the position of 9 mm (around 10% deviation). From the proximal end, the intensity rose dramatically and reached the peak at the positon of 2 mm and then dropped to approximately 80% at the position of 4 mm. The constant intensity was maintained until the position of 9 mm, and a sharp drop in the intensity occurred at the distal end. In the radial direction, Fig. 3b confirms almost isotropic light emission (i.e., normalized intensity = 0.90±0.05). Less than 10% difference was found between the lowest and the highest intensities over 2π. Thus, the laser light was homogenously and cylindrically emitted from the optical diffuser tip in the plane normal to the fiber axis. Preliminary testing also validated no difference in the spatial light distribution between HeNe (632 nm) and 1470 nm wavelengths [20]. The total light transmission was measured to be 81 %.

Figure 4 characterizes the degree of radial compression measured from the fabricated basket device in terms of radial displacement and basket diameter. According to Fig. 4(a), the

radial force linearly increased up to 0.8 N with the radial displacement (up to 4 mm; R^2 = 0.99). Figure 4(b) illustrates radial stiffness K_r as a function of basket diameter. It is noted that the basket became more rigid as compressed into smaller diameters (i.e., compressed state). The maximum stiffness of 0.4 N/mm occurred at the diameter of 2 mm whereas the fully extended state (6 mm in diameter) shows no stiffness.

Figures 5(a) and 5(b) illustrate cross-sectional images of the coagulated liver acquired from the middle position of the tissue after 10-W irradiation for 7 s without (Fig. 5(a)) and with (Fig. 5(b)) using a basket device. The center of the drilled hole is marked as a red dot while a yellow dot indicates the center of the cylindrically coagulated tissue. The irradiation without the aid of the basket ostensibly entailed the offset coagulation along with a coagulation rim of 1.3 ± 0.4 mm (Fig. 5(a)). The maximum temperature measured from the entrance hole surface in the tissue reached up to 90 ± 5 °C. Moreover, no basket condition caused partial carbonization in the middle of the tissue due to a closer distance between the diffuser and the inner tissue surface. In addition, irregular gaps were often associated with higher irradiance and temperature in the tissue, resulting in the eccentric thermal coagulation. On the other hand, the basket-assisted irradiation developed the concentric and uniform coagulation from the inner wall, reflecting the radial emission profile as shown in Fig. 3(b). The coagulation rim was measured to be 1.0 ± 0.1 mm, which was 30% thinner and more consistent than that from no basket condition (i.e., coefficient of variance, CV = 10% for basket condition vs. CV = 31% for no basket condition; $p < 0.001$). The maximum temperature at the entrance hole surface was around 65 ± 4 °C, which was 28% lower than that without using the basket ($p < 0.001$). The basket was thereby able to position the diffuser at the center of the hole in the tissue (at almost equivalent distance), leading to generation of the concentric thermal coagulation. Figure 5(c) demonstrates the quantified eccentricity for both the cases (N = 15 per case). Blue and gray columns represent the eccentricity with and without using the basket device, respectively. The irradiation without the basket resulted in an

eccentricity of 0.62 ± 0.38 mm (maximum eccentricity = 1.4 mm and CV = 61%; yellow lines). On the other hand, the basket-assisted irradiation exhibited a relatively less variant eccentricity of 0.15 ± 0.05 mm (maximum eccentricity = 0.23 mm and CV = 33%; red lines), which is 76% smaller and more consistent (smaller CV) than that from no basket condition ($p < 0.001$). Additionally, e/R_0 was estimated to be 23.7 and 5.5 % for no basket and basket conditions, respectively. The lower e/R_0 from the basket-assisted irradiation confirms that the function of the basket helped the diffusing applicator be invariantly situated at the center of the tissue lumen in order to achieve more circumferential and concentric thermal coagulation in a uniform manner.

Figure 6 exhibits spatial distribution of light emission and absolute temperature measurements without and with tracheal tissue. HeNe application showed that the diffusing light was located along the diffuser axis at the center of the basket arms (Fig. 6(a)), and the entire tissue was homogeneously bright on the active segment of the optical diffuser (Fig. 6(b)). Figure 6(c) presents slight variations in the measured temperature (green solid line) between the nitinol arms and the surrounding temperature (≤ 20 °C), apparently reflecting no or minimal light absorption by the basket arms (minimal temperature increase). However, it was noted that the interface between the head and the distal end of the diffuser experienced a temperature elevation of 26 °C, compared with the middle of the diffuser (24 ^{o}C), possibly due to light absorption by UV curing (lower than melting point). The temperature around the tissue surface (i.e., radial direction; green solid line) was almost constantly maintained at 48±2 °C as shown in Fig. 6(d).

Figure 7(a) shows temporal development of temperature at the middle point on the outer trachea surface (green dot in IR image) under three treatment conditions during *ex vivo* experiment (initial temperature = 20 °C). Although the treatment periods were chosen to be 5 and 10 s, the total recording time was set at 60 s in order to observe the overall temperature tendency during and after the treatment. Regardless of the treatment condition, the overall

temperature sharply increased upon the irradiation but gradually decreased with the time (Fig. 7(a)). The condition of 7 W and 10 s entailed the highest maximum temperature of 89 °C (transient increase rate = 6.9 °C/s), which was 1.4- and 1.8-fold higher than those from the conditions of 10 W and 5 s (maximum temperature = 62 °C and transient increase rate = 8.4 °C/s) and 7 W and 5 s (maximum temperature = 51 °C and transient increase rate = 6.2 °C/s). Thus, it was noted that the higher energy delivery induced the higher maximum temperature in the issue (e.g., 89 °C for 7 W–10 s–70 J vs. 51°C for 7 W–5 s–35 J). In addition, all the conditions were associated with almost comparable transient temperature increase rates. Figure 7(b) presents temperature variations along the longitudinal direction in the tracheal tissue (green solid line in IR image) measured at the end of irradiation. Irrespective of the testing condition**, a temperature discrepancy occurred between proximal and distal ends of the fiber (asymmetric distribution). Both 7 W–5 s–35 J and 10 W–5 s–50 J yielded the differences of around 10 °C and 12 °C between the two ends, respectively. On the other hand, 7 W–10 s–70 J entailed an approximately two-fold higher difference (~20 °C) than the other conditions did (i.e., proximal = 45 °C vs. distal = 65 °C).**

Figure 8 exhibits the dehydration effect of tracheal tissue after photothermal treatment under various conditions. Two conditions of 7 W–5 s–35 J and 10 W–5 s–50 J yielded small changes in spatial shrinkage ratios of 2.2±0.4 and 3.8±0.5 %, respectively. In contrast, 7 W–10 s–70 J resulted in more significant shrinkage due to tissue dehydration with a ratio of 16.5±2.0 %. The phenomenon was clearly observed in histological images as shown in Fig. 9. Figure 9(a) demonstrates the overview of the treated tissue that was circumferentially destroyed. According to Fig. 9(b), the coagulated cell shrinkage resulted from thermal denaturation, contraction of intracellular proteins, and possible collapse of the cytoskeleton [38]. In fact, both the cilia layers and goblet cells were totally ablated (yellow solid arrow) and the pseudostratified columnar epithelium layer was compressed. In addition, the

epithelium layer was eroded and nuclei were disordered (green solid arrow) [39]. A range of the extensive submucosa necrosis (single red arrows) along with vacuolization demonstrated strong dehydration effects during thermal deformation of the tissue structure. Essentially, the increased subsurface heating led to hot pockets of the overheated steam within the tissue. As irradiation duration continued, the hot steam pockets became lager and eventually exploded. In turn, the extracellular vacuole ruptures created the large holes inside the tissue [38].

4. Discussion

The current findings suggest that circumferential and uniform photothermal coagulation on trachea tissue can be achieved by integrating a basket device with a diffusing applicator. As the four arms of the basket were elastic, shape-memorized, symmetric and expandable, the device was firmly in contact with tissue due to its radial pressure on the inner wall. Thus, the diffusing applicator was always held in the center of the tubular trachea, which eventually helped secure consistent thermal denaturation along the circumference. As a consequence, it is conceivable that treatment outcomes would be less dependent on surgeons' skills and experiences. Liver experiments by using 1470-nm laser demonstrated that the treatment dosage (7 W–10 s–70 J) entailed uniform and annular coagulative necrosis (around 1 mm), and the maximum temperature on the tissue hole surface merely reached around 65 °C. Without the basket, a mere diffusing applicator often resulted in eccentric thermal injury and even carbonization due to randomly inconsistent distances. Therefore, the findings from *ex vivo* study can be beneficial for clinical applications in terms of centering the optical devices within the tubular tissue structure. In fact, a number of studies have conducted thermal treatments on the tubular tissue such as urethra, vein, esophagus, and trachea [2, 20, 40, 41]. However, positioning of the device still seems challenging and even critical to determine the clinical outcomes. Although the optical diffuser was developed to deliver laser light radially to treat urethral stricture, the previous study pointed out that out-of-center phenomena

occurred due to blind deployment of the optical diffuser, irregular urethral structure, and lack of centering methods [20]. In addition, various types of fiber tips such bare flat fiber, Tulip-Tip, NeverTouch™, radial fiber, and diffusing fiber were used for endovenous laser ablation (EVLA) for treatment of varicose veins [19, 42]. Nonetheless, without any geometric restraints to prevent the fibers from making contact with vein wall, perforations often occur primarily due to over-heating from unfavorable tissue contact. For tracheal stenosis modelling and treatment, the diffusing applicator was also deployed to induce and evaluate the grade of stenosis developed on rabbit tracheas [2]. The fact remains that the procedures for accurately inserting the fiber into the lumen center were still quite challenging in practice.

According to Fig.4, the proposed basket device confirmed sufficient rigidity to expand the inner diameter of tissue from 5 to 6 mm with a displacement of 1 mm [43]. In other words, the basket shape remained unchanged and the optical diffuser was located at the center of the trachea. On the other hand, radial stiffness (< 0.3 N/mm) at a diameter of 2.4 mm demonstrated that the basket was moderately easy to travel through a plastic tube when it was pushed out or pulled in. Additionally, no damage or injury of a glass cap was observed due to axial tensile stress from four wire arms. However, further tests should be implemented to investigate elastic limits (yield strength or rupture points) of the glass cap to ensure the reliability of the basket for clinical applications.

Despite the fact that 1470 nm laser wavelength was strongly absorbed by water (i.e., primary composition in soft tissue), other materials in the basket device such as nitinol and optical adhesive could absorb the incident wavelength and eventually heat up during the irradiation. As a result, the head part (Fig. 1) absorbed the forwardly transmitted light (around 11% of input power) and reached the temperature of over 50 °C (Fig. 6(c)). As the heated tip was situated in the center and far from the tissue wall, no tissue damage was observed during the current study. Nonetheless, finding the alternative materials with less light absorption will still be taken into consideration for ensuring the safety of the thermal treatment.

Inconsistencies between light emission and the measured temperature profile were noticeable in a radial direction possibly due to irregular wall thickness along the trachea tissue (Figs. 6(b) and 6(d)). **Assuming that the overall light distribution is perfectly cylindrical, one can estimate the irradiance (E; W/cm^2) on the tissue surface (i.e., $E = P / [2\pi r \times l]$), where P = source power (W), r = distance from fiber axis (mm), and l = length of active segment (mm)). The corresponding E for 10 W can thus be estimated to be 4.3 W/cm^2. However, due to the aforementioned inconsistencies, the effect of light intensity distribution on the tissue surface could be dependent upon both optical and thermal profiles. Thus, isotropic probes will be deployed to monitor the real-time light distribution on the mucosal surface of the trachea (around 3 mm away from optical diffuser axis) in the further study [44-47]. The results will then be compared with theoretical analysis of the cylindrical light distribution.** In addition, the temperature discrepancy between the proximal and distal ends became more obvious due to the forward light emission particularly when the treatment period was longer (i.e., 7 W–10 s–70 J) (Fig. 7(b)). Therefore, in order to reduce the inconsistent thermal distribution, the distal tip of a glass cap will be coated by using reflective materials, and further improvement will be made on conical fiber tips.

Although the current study exhibited the feasibility of the proposed basket device to center a diffusing applicator in tubular tissue, experimental limitations still remain. Firstly, a difference in light intensities between proximal and distal ends (Fig. 3(a)) should be minimized to achieve more uniform and cylindrical light distribution along the diffuser axis. Currently, the microscopic evaluations presented relatively wider and deeper holes near the proximal end, which could reduce the probability of light diffusion. The geometrical variations could take place during the longer interaction times particularly when the laser fabrication direction was reversed at the proximal end. Therefore, the current machining system should be upgraded with high precision motor stages and/or high repetition rate pulsed

lasers to achieve smooth boundary transitions and more consistent fabrication outcomes (grooving width, patterning angle, and segment size). Moreover, the diffusing fibers with conical angle tips should be developed by using an acid etching technique to lessen the forward emission and consequently to attain the cylindrical light distribution [20, 48]. Secondly, quantitative evaluations on light absorption by nitinol wire arms are required to ensure no or minimal local thermal injury to the adjacent tissue wall. Thermal-isolating coating will be applied to minimize any undesirable heating effect. Thirdly, IR imaging and measurements only provided temperature information on the outer surface of the tissue, which could be difficult to precisely comprehend light dosimetry and monitoring of the interstitial temperature in practice. In fact, both carbonization in liver and vacuolization in the trachea were undetectable during the IR camera measurements. Moreover, each tracheal structure is heterogeneous and different in each segment due to C-shape of hyaline cartilage. Thus, the integration of temperature sensors (i.e., thermocouple or thermistor) with the proposed basket will be performed to real-time monitor the temperature of the lumen of the trachea during *in vivo* photothermal treatment on rabbit models with trachea stricture. Finally, the working diameter of the proposed optical device was limitedly applicable for specific diameter ranges of the tissue. Thus, a variety of basket design factors (e.g., nitinol material, shape, and tissue lumen size) should be considered to optimize the optical device for further *in vivo* and clinical applications.

For further *in vivo* experiments and clinical translation, two laser parameters should be taken into account: wavelength and irradiation mode. Due to strong light absorption, a modulated 1470-nm laser light will be used to precisely denature or remove fibrotic tissue and to minimize thermal injury to the adjacent tissue (i.e., thin coagulation). Furthermore, to prevent fibrosis recurrence post-treatment, low level laser therapy (LLLT) with 635-nm laser light or administration of anti-fibrosis materials (e.g., fucoidan and phlorotannin) will be evaluated as an adjunctive treatment method in terms of cell proliferation/migration and

myofibroblast transition [49-51]. In addition, various irradiation modes (e.g., pulse duration, duty cycle, and constant energy delivery) will also be attempted to regulate thermal dosimetry and eventually to obtain the predictable coagulation depth.

5. Conclusion

The current study developed the basket-integrated optical device to uniformly treat tubular tissue by centering an optical diffuser in the lumen. Mechanical integrity from the basket arms consistently secured the position of the optical diffuser with minimal temperature increase. Further *in vivo* study will be performed to determine the device design and to identify the optimal therapeutic conditions for treating tracheal stenosis.

Figure legends

Figure 1: Design concept of proposed basket-integrated optical device

Figure 2: Experimental set-up of tracheal tissue testing with basked-integrated optical device (IR: infrared and PL: polarization)

Figure 3: Normalized beam profile of diffusing applicator: (a) longitudinal and (b) radial emissions

Figure 4: Radial compression testing of basket device: (a) radial force at various radial displacements and (b) radial stiffness at various basket diameters

Figure 5. Eccentricity of bovine liver coagulation: cross-sectional tissue images (a) without basket, (b) with basket, and (c) comparison of measured eccentricity

Figure 6. Light emission profile (HeNe laser) (a) without trachea and (b) with trachea and temperature distribution (c) without trachea and (d) with trachea after 7-W 1470-nm irradiation for 5 s (P: proximal and D: distal end). Note that the temperature profiles (blue color) were measured from the green vertical lines in (c) and (d).

Figure 7. Development of temperature in trachea under various conditions: (a) temporal evolution of temperature from middle point of tissue surface (green dot in IR image) and (b) longitudinal temperature distribution on tissue (green solid line in IR image; P: proximal and D: distal end)

Figure 8. Spatial dehydration effect at three different conditions: (a) 7 W – 5 s, (b) 7 W – 10 s, and (c) 10 W – 5 s (P: proximal and D: distal ends; D_i: initial and D_f: final tissue diameters), and (d) comparison of spatial shrinkage ratio ($^{*}p < 0.003$ and $^{**}p < 0.001$).

Figure 9: Histological images of trachea treated at 7 W for 10 s: (a) 10× and (b) 200×

Acknowledgements

This research was supported by a grant of the Korea Health Technology R&D Project through the Korea Health Industry Development Institute (KHIDI), funded by the Ministry of Health & Welfare, Republic of Korea (grant number: HI16C1017).

References

[1] A. T. Hillel, D. Namba, D. Ding, V. Pandian, J. H. Elisseeff, and M. R. Horton, *JAMA Otolaryngol Head Neck Surg*, **140**, 961-966, (2014).
[2] H. S. Lee, S. W. Kim, C. Oak, H. W. Kang, J. Oh, M. J. Jung, S. B. Kim, J. H. Won, and K. D. Lee, *Lasers Surg Med*, 1-8, (2016).
[3] S. Y. Lee, S. M. Lee, S. R. Park, J. W. Chang, T. S. Chung, and H. S. Choi, *Clin Exp Otorhinolaryngol*, **2**, 211, (2009).
[4] Y. Nakagishi, Y. Morimoto, M. Fujita, Y. Ozeki, T. Maehara, and M. Kikuchi, *Laryngoscope*, **115**, 1087-1092, (2005).
[5] S. Saenghirunvattana, V. Pitiguagool, C. Suwanakijboriharn, P. Pupipat, B. Saenghirunvattana, M. C. Gonzales, K. Sutthisri, C. Siangproh, W. Kodkaew, and A. Inkum, *OJRD*, **2014**, (2014).
[6] A. Gelbard, D. O. Francis, V. C. Sandulache, J. C. Simmons, D. T. Donovan, and J. Ongkasuwan, *Laryngoscope*, **125**, 1137-1143, (2015).
[7] R. Farzanegan, B. Farzanegan, M. Zangi, M. G. Eraghi, S. Noorbakhsh, N. D. Tabarestani, and M. B. Shadmehr, *Iran Red Crescent Med J*, **18**, (2016).
[8] S. H. Oh, S. J. Lee, D. S. Kim, M. J. Na, E. Choi, S. J. Kwon, H. M. Cho, and J. W. Son, *Tuberc Respir Dis*, **75**, 79-82, (2013).
[9] A. Dass, N. M. Nagarkar, S. K. Singhal, and H. Verma, *Iran J Otorhinolaryngol*, **26**, 37, (2014).
[10] C. Witt, B. Schmidt, J. Llebetruth, and G. Baumann, *Lasers Surg Med*, **20**, 51-55, (1997).
[11] H. S. Lee, S. W. Kim, C. Oak, Y. C. Ahn, H. W. Kang, B. K. Chun, and K. D. Lee, *Int J Pediatr Otorhinolaryngol*, **79**, 2384-2388, (2015).
[12] G. Marulli, G. Rizzardi, L. Bortolotti, M. Loy, C. Breda, A. M. Hamad, F. Sartori, and F. Rea, *Interact Cardiovasc Thorac Surg*, **7**, 227-230, (2008).
[13] M. G. Saueressig, A. V. d. Macedo Neto, J. d. O. Espinel, M. I. Edelweiss, P. R. S. Sanches, and R. G. Xavier, *Rev. Col. Bras. Cir.*, **38**, 412-416, (2011).
[14] W. Gesierich, F. Reichenberger, A. Fertl, K. Haeussinger, and R. Sroka, *J Thorac Cardiovasc Surg*, **147**, 1827-1832, (2014).
[15] A. Brichet, C. Verkindre, J. Dupont, M. Carlier, J. Darras, A. Wurtz, P. Ramon, and C. Marquette, *Eur Respir J Suppl*, **13**, 888-893, (1999).
[16] A. Gomez-Caro, A. Morcillo, R. Wins, L. Molins, G. Galan, and V. Tarrazona, *Multimed Man Cardiothorac Surg*, **2011**, 4945, (2011).
[17] A. F. Gelb, and J. D. Epstein, *West J Med*, **141**, 472, (1984).
[18] T. Inouye, T. Tanabe, M. Nakanoboh, Y. Ohmae, and M. Ogura, *J Clin Laser Med Surg*, **12**, 97-101, (1994).
[19] M. Ahn, Y. G. Chae, J. Hwang, Y. C. Ahn, and H. W. Kang, *J Biophotonics*, **11**, 1-11, (2016).
[20] T. H. Nguyen, Y. H. Rhee, J. C. Ahn, and H. W. Kang, *Optics express*, **23**, 20829-20840, (2015).
[21] B. Freitag, R. Sroka, S. Koelle, A. Becker, W. Khoder, T. Pongratz, C. Stief, and M. Trottmann, *Proc. SPIE*, **8926**, 89261C-89261C-89263, (2014).
[22] M. Panjehpour, B. F. Overholt, R. C. Denovo, R. E. Sneed, and M. G. Petersen, *Lasers Surg Med*, **12**, 631-638, (1992).
[23] B. F. Overholt, M. Panjehpour, R. C. Denovo, and M. G. Petersen, *Lasers Surg Med*, **14**, 27-33, (1994).
[24] B. F. Overholt, M. Panjehpour, R. C. DeNovo, M. G. Peterson, and C. Jenkins, *Lasers Surg Med*, **18**, 248-252, (1996).
[25] D. Stöckel, *New Developments in Forming Technology*, 119-134, (2001).
[26] L. Petrini, and F. Migliavacca, *Journal of Metallurgy*, **2011**, (2011).

[27] W. Cwikiel, R. Willen, H. Stridbeck, R. Lillo-Gil, and C. S. von Holstein, *Radiology*, **187**, 667-671, (1993).
[28] K. Yanagihara, H. Mizuno, H. Wada, and S. Hitomi, *Ann Thorac Surg*, **63**, 1786-1789, (1997).
[29] M. Pocek, F. Maspes, S. Masala, E. Squillaci, G. Assegnati, A. Moraldi, and G. Simonetti, *European radiology*, **6**, 230-235, (1996).
[30] S. Thompson, *Int Endod J*, **33**, 297-310, (2000).
[31] Y. Kaieda, *Sci Tech Adv Mater*, **4**, 239-246, (2003).
[32] C. Trepanier, T. Leung, M. Tabrizian, L. H. Yahia, J. G. Bienvenu, J. F. Tanguay, D. Piron, and L. Bilodeau, *J Biomed Mater Res A* **48**, 165-171, (1999).
[33] B. Thierry, Y. Merhi, L. Bilodeau, C. Trepanier, and M. Tabrizian, *Biomaterials*, **23**, 2997-3005, (2002).
[34] J. Ryhänen, *Minim Invasive Ther Allied Technol*, **9**, 99-105, (2000).
[35] D. Vojtěch, *Czech Academy of Science*, (2010).
[36] G. J. Müller, and A. Roggan, Laser-induced interstitial thermotherapy, *SPIE*, Washington, (1995).
[37] FLIR A3xx pt series - User's Manual, *FLIR Systems*, California, (2014).
[38] S. Thomsen, *Photochem Photobiol*, **53**, 825-835, (1991).
[39] A. J. Osborn, R. Chami, E. J. Propst, I. Luginbuehl, G. Taylor, J. A. Fisher, and V. Forte, *Laryngoscope*, **123**, 2742-2748, (2013).
[40] X. B. D'Journo, and P. A. Thomas, *J Thorac Dis*, **6**, 253-264, (2014).
[41] R. Sroka, K. Weick, M. Sadeghi‐Azandaryani, B. Steckmeier, and C. G. Schmedt, *J Biophotonics*, **3**, 269-276, (2010).
[42] T. Stokbroekx, A. de Boer, R. M. Verdaasdonk, M. E. Vuylsteke, and S. R. Mordon, *Lasers Med Sci*, **29**, 501-507, (2014).
[43] M. C. Jones, F. A. Rueggeberg, H. A. Faircloth, A. J. Cunningham, C. M. Bush, J. D. Prosser, J. L. Waller, G. N. Postma, and P. M. Weinberger, *Laryngoscope*, **124**, 2352-2358, (2014).
[44] C. Munck, S. Mordon, and N. Betrouni, *Photodiagnosis Photodyn Ther* **16**, 23-26, (2016).
[45] H. J. Van Staveren, H. P. Marijnissen, M. C. Aalders, and W. M. Star, *Lasers Med Sci*, **10**, 137-147, (1995).
[46] R. L. van Veen, M. C. Aalders, K. L. Pasma, P. D. Siersema, J. Haringsma, W. Van de Vrie, E. E. Gabeler, D. J. Robinson, and H. J. Sterenborg, *Lasers Surg Med*, **31**, 299-304, (2002).
[47] M. De Jode, *Phys. Med. Biol*, **44**, 3027, (1999).
[48] N. T. Pham, S. L. Lee, S. Park, Y. W. Lee, and H. W. Kang, *J Biomed Opt*, **22**, 045008-045008, (2017).
[49] C. Sassoli, F. Chellini, R. Squecco, A. Tani, E. Idrizaj, D. Nosi, M. Giannelli, and S. Zecchi‐Orlandini, *Lasers Surg Med*, **48**, 318-332, (2016).
[50] M. Xue, Y. Ge, J. Zhang, Q. Wang, L. Hou, Y. Liu, L. Sun, and Q. Li, *PLoS one*, **7**, e43483, (2012).
[51] M. M. Kim, Q. Van Ta, E. Mendis, N. Rajapakse, W. K. Jung, H. G. Byun, Y. J. Jeon, and S. K. Kim, *Life Sci*, **79**, 1436-1443, (2006).

Figure 1. Design concept of proposed basket-integrated optical device

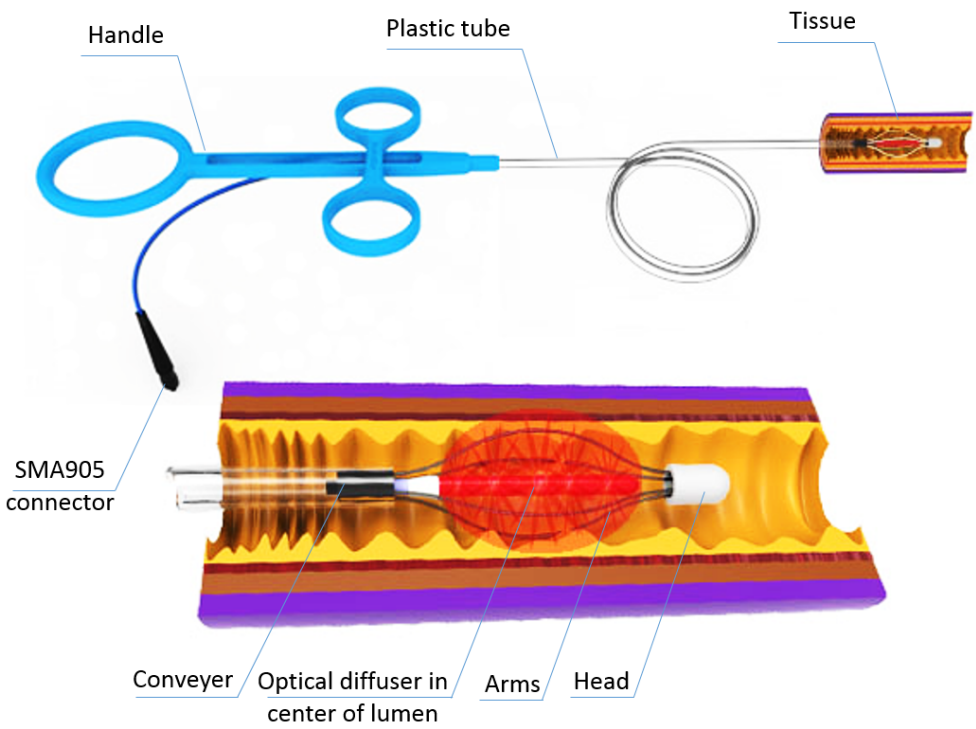

Figure 2. Experimental set-up of tracheal tissue testing with basked-integrated optical device (IR: infrared and PL: polarization)

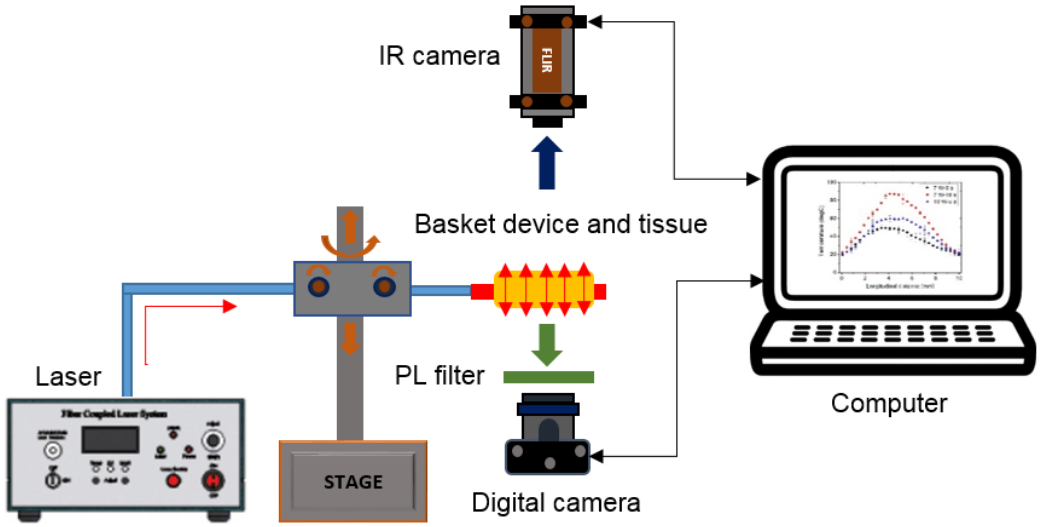

Figure 3. Normalized beam profile from diffusing applicator: (a) longitudinal and (b) radial emissions

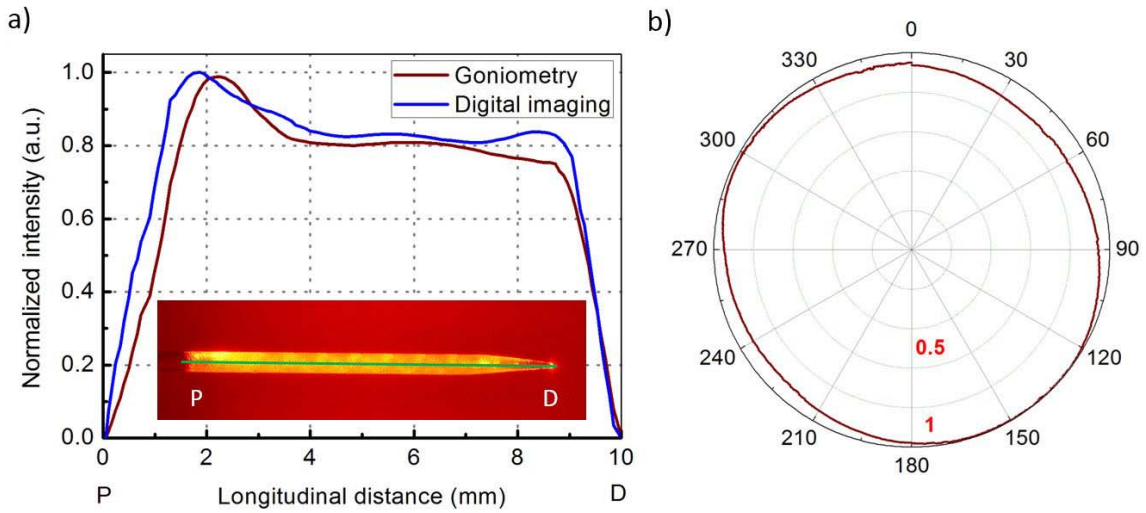

Figure 4. Radial compression testing of basket device: (a) radial force at various radial displacements and (b) radial stiffness at various basket diameters

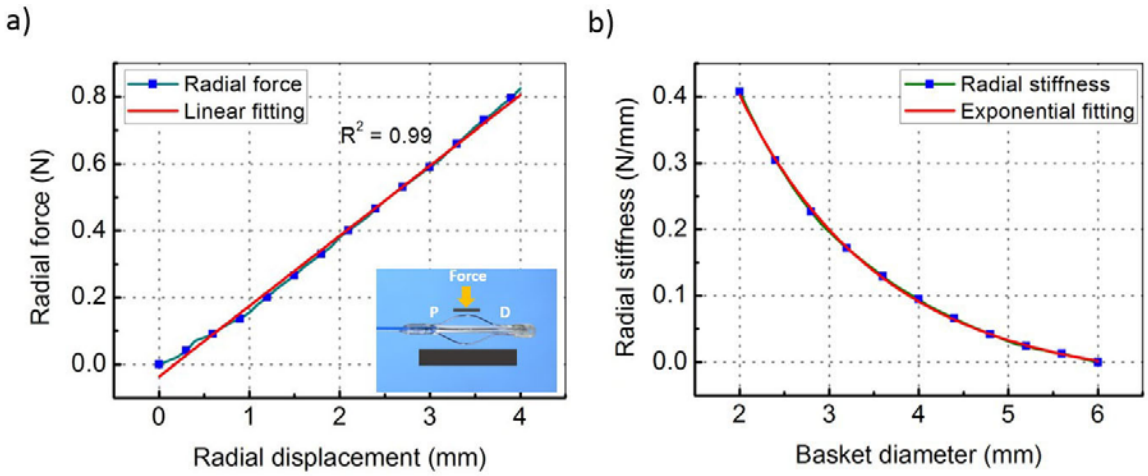

Figure 5. Eccentricity of bovine liver coagulation: cross-sectional tissue images (a) without basket, (b) with basket, and (c) comparison of measured eccentricity

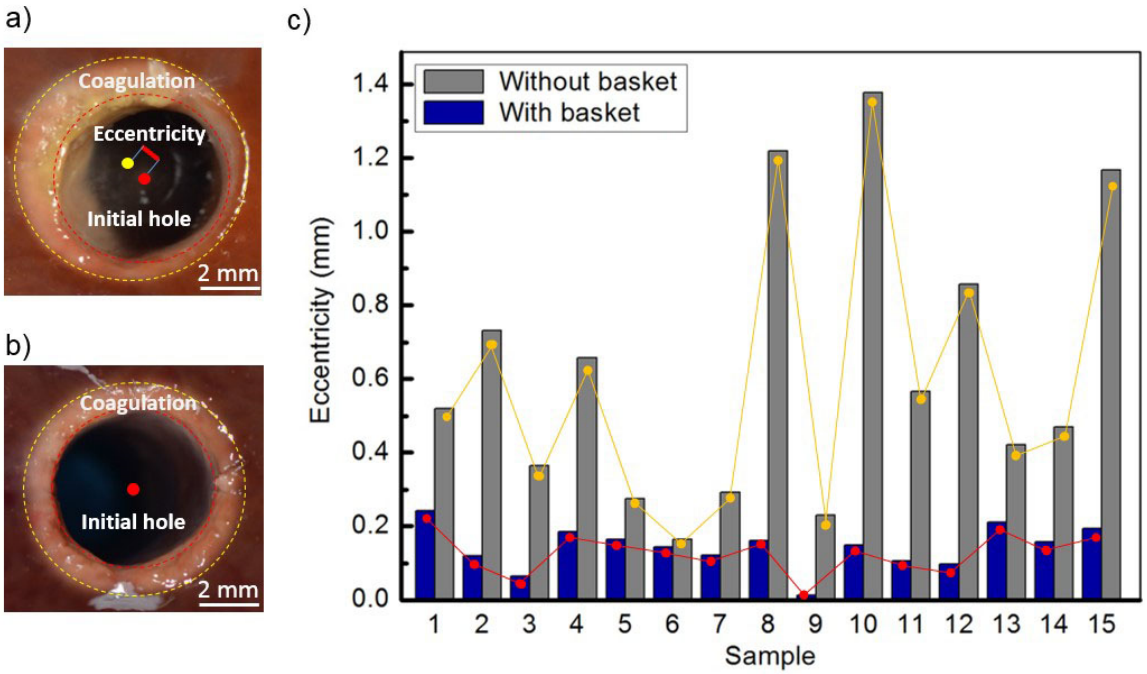

Figure 6. Light emission profile (HeNe laser) (a) without trachea and (b) with trachea and temperature distribution (c) without trachea and (d) with trachea after 7-W 1470-nm irradiation for 5 s (P: proximal and D: distal end). Note that the temperature profiles (blue color) were measured from the green vertical lines in (c) and (d).

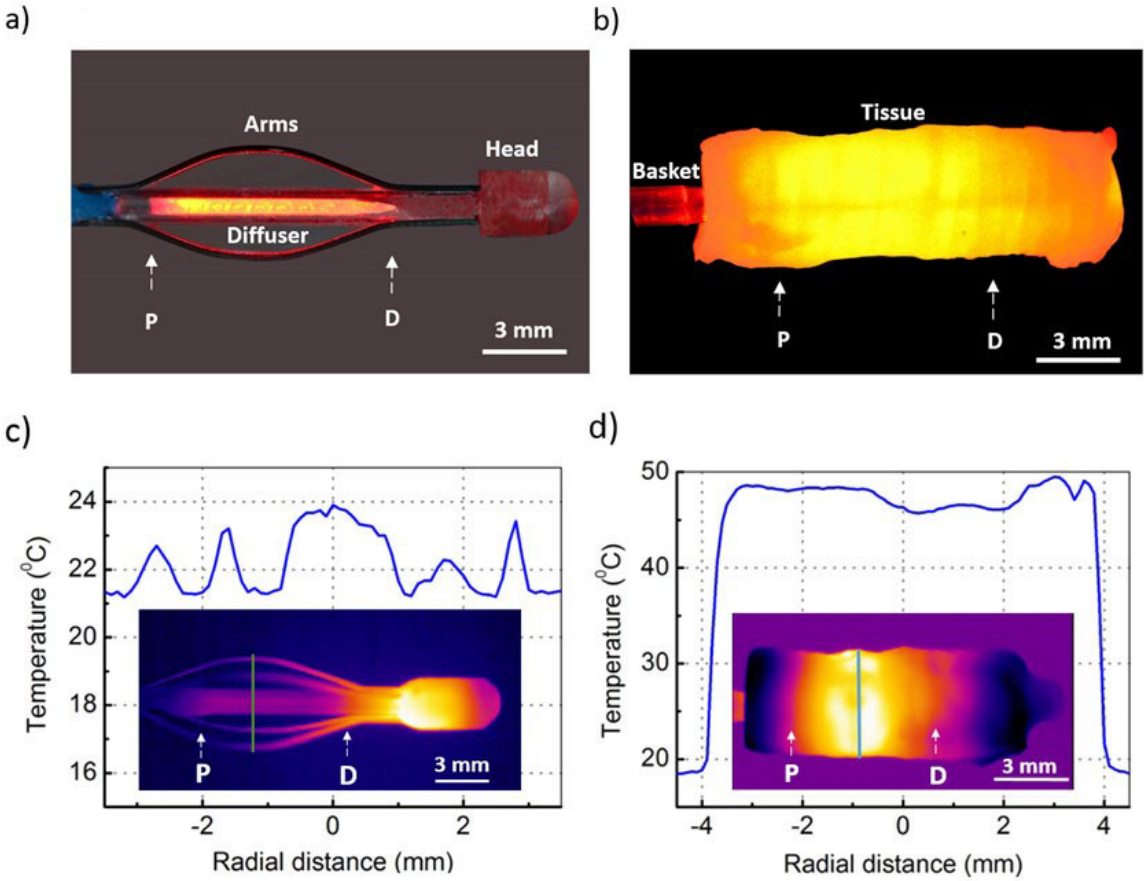

Figure 7. Development of temperature in trachea under various conditions: (a) temporal evolution of temperature from middle point of tissue surface (green dot in IR image) and (b) longitudinal temperature distribution on tissue (green solid line in IR image; P: proximal and D: distal end)

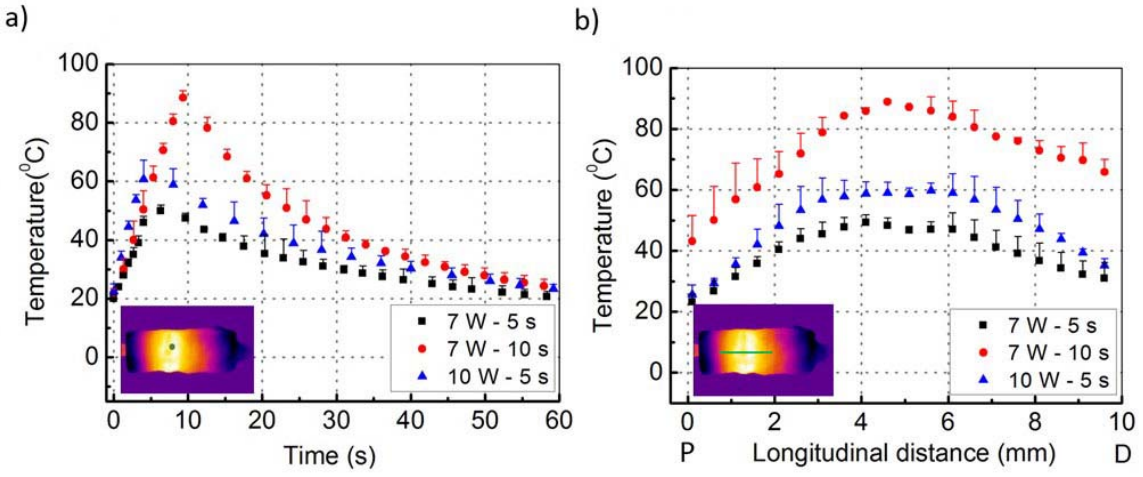

Figure 8. Spatial dehydration effect at three different conditions: (a) 7 W – 5 s, (b) 7 W – 10 s, and (c) 10 W – 5 s (P: proximal and D: distal ends; D_i: initial and D_f: final tissue diameters), and (d) comparison of spatial shrinkage ratio ($^{*}p < 0.003$ and $^{**}p < 0.001$).

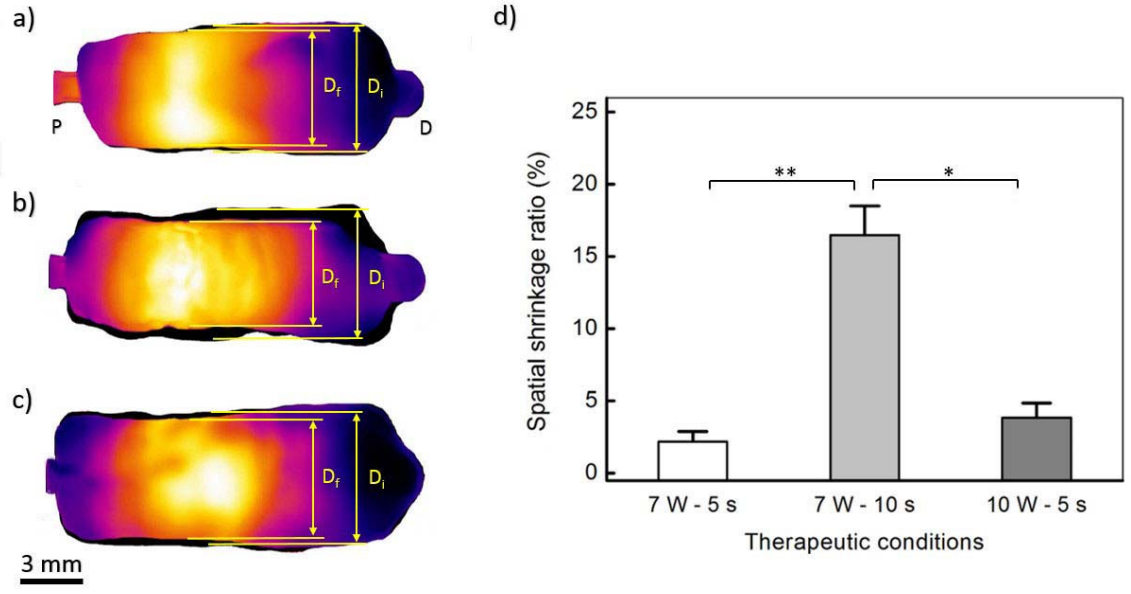

Fig. 9. Histological images of trachea treated at 7 W for 10 s: (a) 10× and (b) 200×